Characterization of escape times of Josephson junctions for signal detection

Paolo Addesso,[1] Giovanni Filatrella,[2] and Vincenzo Pierro[3]

[1]*Department of Electrical Engineering and Information Engineering, Via Ponte Don Melillo, 1, I-84084 Fisciano, Italy*
[2]*Department of Sciences for Biological, Geological, and Environmental Studies, University of Sannio, Via Port'Arsa,*
11, I-82100 Benevento, Italy
[3]*Department of Engineering, University of Sannio, Corso Garibaldi, 107, I-82100 Benevento, Italy*

The measurement of the escape time of a Josephson junction might be used to detect the presence of a sinusoidal signal embedded in noise when use of standard signal processing tools can be prohibitive due to the extreme weakness of the source or to the huge amount of data. In this paper we show that the prescriptions for the experimental setup and some physical behaviors depend on the detection strategy. More specifically, by exploitation of the sample mean of escape times to perform detection, two resonant regions are identified. At low frequencies there is a stochastic resonance or activation phenomenon, while near the plasma frequency a geometric resonance appears. Furthermore, detection performance in the geometric resonance region is maximized at the prescribed value of the bias current. The naive sample mean detector is outperformed, in terms of error probability, by the optimal likelihood ratio test. The latter exhibits only geometric resonance, showing monotonically increasing performance as the bias current approaches the junction critical current. In this regime the escape times are vanishingly small and therefore performance is essentially limited by measurement electronics. The behavior of the likelihood ratio and sample mean detector for different values of incoming signal to noise ratio is discussed, and a relationship with the error probability is found. Detectors based on the likelihood ratio test could be employed also to estimate unknown parameters in the applied input signal. As a prototypical example we study the phase estimation problem of a sinusoidal current, which is accomplished by using the filter bank approach. Finally we show that for a physically feasible detector the performances are found to be very close to the Cramer-Rao theoretical bound. Applications might be found, for example, in some astronomical detection problems (where the all-sky gravitational and/or radio wave search for pulsars requires the analysis of nearly sinusoidal long-lived waveforms at very low signal-to-noise ratio) or to analyze weak signals in the subterahertz range (where the traditional electronics counterpart is difficult to implement).

I. INTRODUCTION

Threshold detection [1,2] is based on the possibility of ascertaining the presence of a signal via the transition from one metastable state to another. Thus, the essential ingredients are (i) a two-state detector, (ii) a switch from one state to the other induced by the signal, and (iii) the possibility of detecting the transitions when the detector observable crosses a threshold. Under such conditions the original signal is transformed into a series of time intervals, i.e., the residence times in each state.

From the physical point of view, the joint action of the applied external signal and the fluctuations induces an escape from a metastable state of the detector. The distribution of the escapes acquires, under very general assumptions, the shape of an activation law like the Arrhenius law with an effective energy barrier that depends upon the fluctuation spectrum and the signal (or perturbation) shape [3–5]. The general idea beyond threshold detectors is that, in view of the exponential character of the activation law, residence times are very sensitive to small signals. Analysis of escape time series entails a loss of information with respect to the direct signal observation. Conversely, it may be useful to reduce the amount of data to be analyzed. In this perspective, threshold detection has been examined through the lens of information theory [6] and/or signal processing [7,8].

In this paper we propose to characterize underdamped Josephson junctions (JJs) as detectors based on the statistics of the escape times. It is well known that JJs are superconducting elements that can operate at extremely low temperatures (as low as refrigeration allows) and hence they are affected by a low intrinsic noise. Let us remark that to take advantage of the speed and low noise features of JJs it is necessary to analyze escape times, inasmuch as the dynamics of the Josephson phase is not directly observable. Instead, the escape from the metastable static solution causes a voltage step, associated with the average phase derivative, that is actually detectable.

Starting from the pioneering papers of Refs. [9,10], a lot of experimental work has been performed on the role of noise in ac-driven JJs to detect the phase of the applied signal [11], to study quantum computation [12] or ratchet effects [13]. Another remarkable topic is related to employment of a JJ as a threshold detector to characterize (up to higher-order moments) weak fluctuations close to the quantum limit [14–17] (albeit there is also some controversial discussion about the role of quantum noise in JJs [18]). In the ac-driven quantum regime [19] the use of JJs is particularly appealing for signal detection, since ways have been devised to minimize the environmental disturbances to the unavoidable quantum level [20].

JJ-based detection schemes are very interesting for the applications when the source is so weak that an intermediate amplification stage can introduce too much undesirable noise. Indeed, superconducting quantum interference devices (SQUIDs) [21] are sensitive to magnetic flux that is a fraction of the quantum flux, $\Phi_0 \sim 10^{-15}$ Wb. The operating frequency range (up to the terahertz time scale)

is another appealing feature of JJs. In this connection it can be argued that interesting applications are in the field of terahertz sensing and in analog processing [22]. Another remarkable potential application is related to the search for gravitational wave sources where standard signal processing techniques (i.e., matched filters), essentially based on the intensive use of fast Fourier transform (FFT) algorithms, are computationally prohibitive because applied to a large amount of data characterized by a very small signal-to-noise ratio (SNR) [23]. We remark that these examples are merely suggestive because our analysis is a proof of principle, not a careful examination of the applications and of the technical problems.

It should also be noted that a lot of theoretical problems concerning the proposed dynamical system are currently under study. Indeed, a resonant behavior, which can further improve detection, is expected to occur when the time scale of the external signal matches the fluctuation-induced escape time [24]. Thus JJs are also a playground for topics of active research such as stochastic resonance [25] or stochastic activation [26–28] that could arise in such a scenario.

The purpose of this paper is to provide a characterization of the JJ as a detector of a periodic signal. The aim is to show that nonlinear analog processing, for example to apply the signal to a JJ, might represent a viable alternative. In fact the signal could be applied and processed at very high frequency (for JJs are very fast electronic devices) and with very little extra noise from the nonlinear device (for JJs are superconducting elements that work also at very low temperatures).

It has been proven that a simple statistical analysis of JJ output, such as the sample mean (SM) of transition times, could detect the presence of a sinusoid embedded in thermal noise [29]. A more effective analysis of the transition times can be performed by means of appropriate methods of statistical signal processing [30,31], such as the likelihood ratio test (LRT). As expected, LRT performances depend upon a suitable selection of the physical JJ parameters. The lack of analytical results for the escape time distribution in the so-called underdamped case compels us to use extensive numerical simulations in order to search for the JJ optimal working point in a feasible range of the relevant parameters.

The paper is organized as follows: In Sec. II we briefly describe the physical model of the periodically driven JJ that determines the escape times. In Sec. III we describe the statistical tools used to analyze the escape times, while some technical details are deferred to the Appendixes. In Sec. IV we present numerical results that clarify the effectiveness of the statistical analysis, for both signal detection and parameter estimation, namely, the sinusoidal phase. Moreover we perform the JJ physical parameter optimization in order to further improve the detection of a perfectly known sinusoidal signal. Section V is devoted to the conclusions.

II. ESCAPE TIME DISTRIBUTION: PHYSICAL MODEL AND MOTIVATION

A JJ biased with a sinusoidal signal of amplitude S_0 and corrupted by additive noise $\xi(t)$ is modeled by the Langevin

equation [32]

$$\frac{C\hbar}{2e}\frac{d^2\varphi}{dt^2} + \frac{\hbar}{R2e}\frac{d\varphi}{dt} + I_c\sin(\varphi)$$
$$= I_B + S_0\sin(\Omega t + \varphi_0) + \sqrt{D}\xi(t) + \sqrt{k_bT/R}n(t). \quad (1)$$

Here C and R are the capacitance and the resistance of the JJ, respectively (we consider the JJ in the underdamped regime, because the capacitance is not negligible). Furthermore, I_c denotes the Josephson critical current, while I_B is the bias current, k_b denotes the Boltzmann constant, and T is the JJ temperature. The terms $\xi(t)$ and $n(t)$ are white Gaussian noise stochastic variables, whose correlators read $\langle n(t)n(t')\rangle = 2\delta(t - t')$ and $\langle \xi(t)\xi(t')\rangle = 2\delta(t - t')$.

In Eq. (1) thermal fluctuations $\sqrt{k_bT/R}$ can be neglected with respect to the signal noise D if $T \ll DR/k_b$. In fact JJs can be cooled down to a temperature T much below the signal noise temperature; thus in the rest of the paper we will assume that the stochastic component is dominated by the signal fluctuations of intensity D. The condition allowing neglect of thermal fluctuations is favored when the junction resistance is high, i.e., when dissipation is low, for Eq. (1) is based on a parallel lumped circuit model (see the inset of Fig. 1). In Sec. IV B we will show that low dissipation also favors detection, thus reinforcing the advantages of high R.

Introducing the dimensionless time $\tau = \omega_j t$, normalized with respect to the characteristic frequency (called the Josephson frequency) $\omega_j = [2eI_c/(\hbar C)]^{1/2}$, and rearranging the terms, the equation in the aforementioned approximation reads

$$\frac{d^2\varphi}{d\tau^2} + \frac{\omega_j}{RI_c}\frac{\hbar}{2e}\frac{d\varphi}{d\tau} + \sin(\varphi)$$
$$= \frac{I_B}{I_c} + \frac{S_0}{I_c}\sin\left(\frac{\Omega}{\omega_j}\tau + \varphi_0\right) + \frac{S_N}{I_c}\tilde{\xi}(\tau). \quad (2)$$
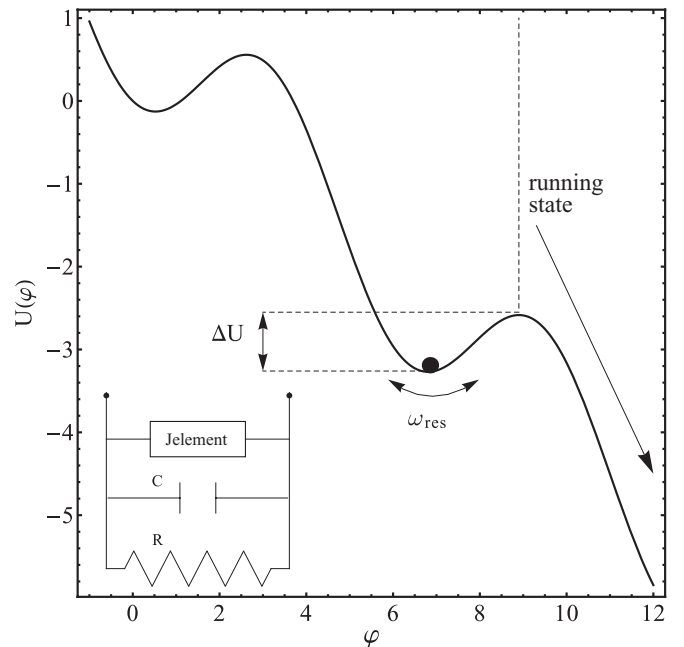

FIG. 1. Schematic of the escape process. The junction switches over the energy barrier ΔU and gives rise to a voltage signal in the running state. The inset shows the electric circuit model of Eq. (1).

In Eq. (2) we have defined $S_N = \sqrt{\omega_j D}$ as the intensity of the noise current, while the correlator in these normalized units reads

$$\langle \tilde{\xi}(\tau)\tilde{\xi}(\tau')\rangle = 2\delta(\tau - \tau'). \tag{3}$$

With the definitions $\gamma = I_B/I_c$ as the normalized bias current, $\alpha = (\omega_j/RI_c)(\hbar/2e)$ as the normalized dissipation, $\varepsilon = S_0/I_c$ as the normalized signal amplitude, and $\varepsilon_N = (S_N/I_c)^2$ as the normalized noise intensity, Eq. (2) reads

$$\frac{d^2\varphi}{d\tau^2} + \alpha\frac{d\varphi}{d\tau} + \sin(\varphi) = \gamma + \varepsilon\sin(\omega\tau + \varphi_0) + \sqrt{\varepsilon_N}\tilde{\xi}(\tau). \tag{4}$$

A washboard potential is associated with Eq. (4) that, for $\gamma < 1$, gives rise to a barrier [33]

$$\Delta U(\gamma) = 2[\sqrt{1-\gamma^2} - \gamma\cos^{-1}(\gamma)]. \tag{5}$$

The schematic of the physics of the device is depicted in Fig. 1 as a jump over an activation barrier. When the system overcomes the energy barrier ΔU, it switches from the locked state to a running state that is associated with a finite voltage [34]; hence it is possible to measure the escape time [35]. For overdamped JJs the voltage step is very smooth, and it is difficult to define the escape from the local solution. Therefore the detection efficiency of overdamped JJs drops down.

The main idea of signal detection is to collect the escape times to discriminate between two situations: (i) the exit is caused by the presence of pure noise (no signal is present, $S_0 = 0$); (ii) the exit is caused by the joint action of noise and
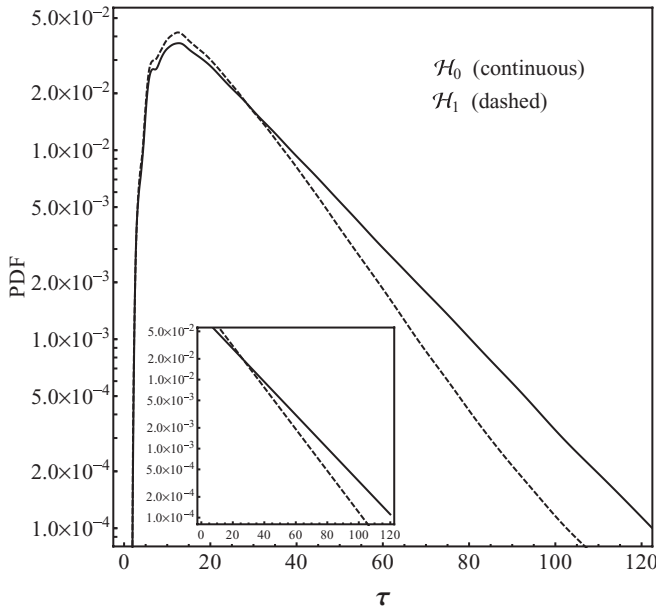

FIG. 2. Distribution of the escape times with (dashed line) and without (continuous line) the sinusoidal signal. The main effect of the signal for this range of the parameters is to change the slope of the distribution. The inset shows the asymptotic fit with exponential distributions. The resulting decay rate in the presence of (without) the signal is 0.069 (0.055). Parameters of the simulations are $\gamma = 0.5$, $\alpha = 0.05$, and $\varepsilon_N = 0.07$. Moreover, when the signal is present, $\varepsilon = 0.1$, $\varphi_0 = 0$, and $\omega = 0.035$.
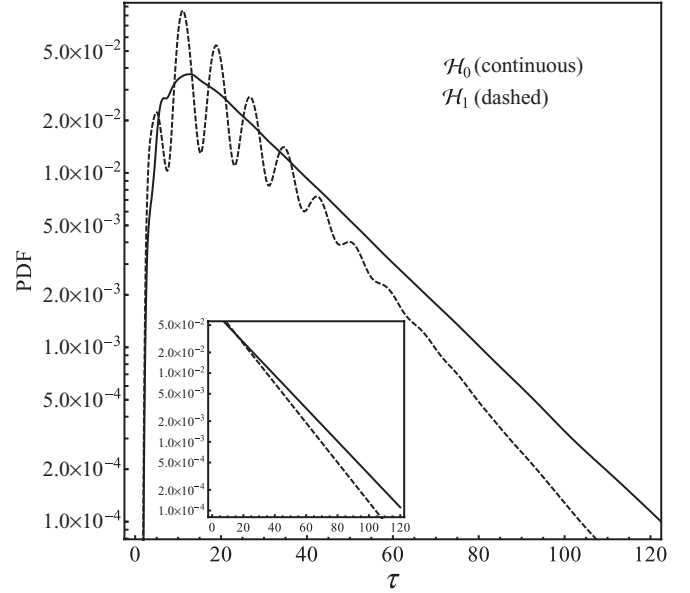

FIG. 3. Distributions of the escape times with (dashed line) and without (continuous line) the sinusoidal signal. The main effect of the signal for this range of the parameters is to introduce oscillations in the escape time distribution. The inset shows the asymptotic fit with exponential distributions. The resulting decay rate in the presence of (without) the signal is 0.066 (0.055). Parameters of the simulations are $\gamma = 0.5$, $\alpha = 0.05$, and $\varepsilon_N = 0.07$. Moreover, when the signal is present, $\varepsilon = 0.1$, $\varphi_0 = 0$, and $\omega = 0.8$.

a sinusoidal excitation (the signal is present, $S_0 \neq 0$). Indeed, escape time distributions are highly sensitive to the signal amplitude, as shown since the pioneering experiments [10]. Typical escape time probability density functions (PDFs) are shown in Figs. 2 and 3 for two different sets of parameters. The random sequence of escape times is obtained by numerical integration of the stochastic differential equation (4), accumulating the first-passage time to cross the maximum of the potential barrier (5), and taking into account the corrections of Ref. [36].

The solid line denotes the escape time without signal ($S_0 = 0$) and the dashed line denotes the escape aided by a sinusoidal forcing ($S_0 \neq 0$). A possible signal detection strategy based on the sample mean of the escape times [29] measures only the average escape time, which is essentially the slope shown in the inset of Figs. 2 and 3. On the other hand, Fig. 3 makes it clear that the two distributions (with and without the sinusoidal signal) are, for some parameter values, very different in shape, not just in the mean value. This difference in shape is exploited in Sec. III, where it is shown that a more refined analysis can lead to better performances for signal detection. Moreover, in Fig. 4 the effect of the signal (initial) phase is shown. The drastic change in the distribution form, while the slope remains almost constant, again demonstrates the need of a more refined analysis, to achieve signal phase estimation by using the escape times, as discussed in Sec. IV C.

The escape time distribution depends not only upon the signal, but also on the physical JJ features. The JJ parameters that can be set in experiments to achieve best detection are the
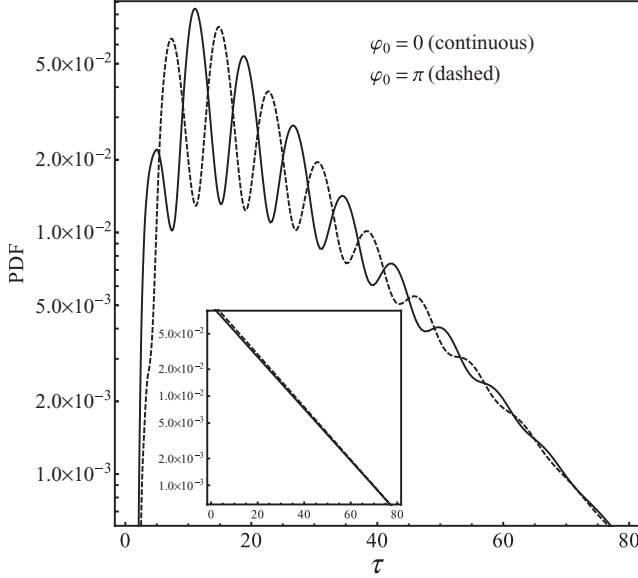
FIG. 4. Distributions of the escape times with a signal with two initial phases, $\varphi_0 = 0$ and $\varphi_0 = \pi$. The inset shows the asymptotic fit with exponential distributions; it is evident that the exponential decay rate is almost the same. Indeed the resulting decay rate for $\phi_0 = 0$ ($\phi_0 = \pi$) is 0.067 (0.068). The other parameters of the simulations are $\gamma = 0.5$, $\alpha = 0.05$, $\varepsilon_N = 0.07$, $\varepsilon = 0.1$, and $\omega = 0.8$.

electrical characteristics of the physical JJ (C, R, I_c) and the external bias current I_B. Moreover, if the signal is recorded, the speed at which the recorded signal $S(t)$ is physically applied is also a tunable parameter. A blind search in such a multidimensional parameter space would be numerically prohibitive and of little physical significance; we therefore discuss in Sec. IV the physical meaning of the parameters to restrict the plausible region in which to seek for best performances.

III. STRATEGIES FOR JJ THRESHOLD DETECTION

The JJ activation energy barrier defined in Eq. (5) refers to an unperturbed junction, i.e., to the case $S_0 = 0$ in Eq. (4). The addition of a deterministic sinusoidal signal of amplitude S_0 results in an oscillation of the barrier that affects the average escape time. The deviations of such an average escape time shown in Figs. 2 and 3 can be used to infer the presence of a signal. Inspection of Figs. 2 and 3 discloses an evident exponential decay of the escape time distribution. This behavior has been previously exploited (see, Ref. [29]) with a straightforward SM detection strategy based on the mean escape time. Indeed, it can be shown that if the escape times are exponentially distributed in both cases $S_0 = 0$ and $S_0 \neq 0$, then the SM detection strategy is an optimal strategy [31]. In the same paper [29] the Kumar-Carrol (KC) index d_{KC} [37] for different SNRs (we recall that the SNR is related to the ratio $S_0/S_N = S_0/\sqrt{\omega_j D}$) has been used as a simple (heuristic) indicator of the detector performances. We recall that the index d_{KC} depends upon the operating frequency of the applied signal and the extrema are influenced by the noise intensity [11,29], a peculiarity of stochastic resonance [25,38].

When the PDFs are not exponential (and not explicitly known, as is the case for underdamped JJs), we use an accurate and fairly common technique to determine a detection strategy and the related detector, both based on likelihood maximization. Such a decision criterion, based on the LRT, is optimal [31] in a sense that is clarified below. Detectors based on the LRT employ the knowledge of the full probability distributions of the random escape with and without the signal; therefore the shape of PDFs can be properly handled to improve the performances.

Unfortunately, the escape time distributions are not theoretically known for the system described by Eq. (4). Even in the case $S_0 = 0$ the Arrhenius law is approximately valid for rare escapes [9] (in the unperturbed oscillator time scale ω_j), while for fast escapes [39] (which are interesting for signal analysis) only approximated analytical estimates exist. When the signal is applied the knowledge of the escape time distributions is even poorer, and essentially limited to the overdamped case [40]. Our solution is based on a semianalytical approach, so that the analytical results are used as a guess for a numerical procedure. In the following we describe the proposed LRT embedded in the general framework of statistical decision theory.

A. Statistical decision theory and LRT detector

To properly define the detection strategies, it is usual to formalize the problem as a binary hypothesis test:

$$\mathcal{H}_0: \quad \text{sinusoidal signal is absent,}$$
$$\mathcal{H}_1: \quad \text{sinusoidal signal is present.}$$

For this decision problem two different error probabilities arise:

(a) the *false alarm probability* P_f, also called type I error probability, i.e., the probability to decide for the hypothesis $\mathcal{H}_1$ when $\mathcal{H}_0$ is true;

(b) the *miss probability* P_m, also called type II error probability, i.e., the probability to decide for the hypothesis $\mathcal{H}_0$ when $\mathcal{H}_1$ is true.

We start by considering the case in which the JJ normalized parameters (α and γ) and the normalized noise standard deviation ε_N are perfectly known and do not depend on the particular hypothesis in force. We also assume that the signal parameters (i.e., ε, ω, and φ_0) are known under the $\mathcal{H}_1$ hypothesis. In this setup the Neyman-Pearson lemma [30] identifies the LRT as the optimal detection strategy, for it minimizes, among all possible tests, the miss probability P_m at a fixed false alarm level P_f. Thus if we collect N escape times $\boldsymbol{\tau} = \{\tau_i\}_{i \in [1,N]}$, supposed to be independent and identically distributed, the test statistic can be written as

$$\prod_{i=1}^{N} \frac{f_1(\tau_i)}{f_0(\tau_i)} \underset{\mathcal{H}_0}{\overset{\mathcal{H}_1}{\underset{<}{\gtrless}}} \zeta', \tag{6}$$

where $f_{0,1}(\cdot)$ are the PDFs of the escape times under the hypothesis $\mathcal{H}_{0,1}$, while ζ' is a suitable threshold selected to return a fixed false alarm level. To simplify the computation of the statistic (6), it is possible to compare the normalized

natural logarithm of the likelihood ratio with a threshold $\zeta = \ln(\zeta')/N$:

$$\Lambda(\boldsymbol{\tau}) = \frac{1}{N} \sum_{i=1}^{N} \ln \left[\frac{f_1(\tau_i)}{f_0(\tau_i)} \right] \mathop{\substack{\mathcal{H}_1 \\ > \\ < \\ \mathcal{H}_0}} \zeta. \tag{7}$$

The advantage of Eq. (7) is that the statistic $\Lambda(\boldsymbol{\tau})$ can be computed as the sample mean of the random samples $\mathcal{L} = \{\mathcal{L}_i\}_{i \in [1,N]}$ that are obtained from the escape times via the *optimal* (in the Neyman-Pearson sense) nonlinearity

$$\mathcal{L}_i = \ln \left[\frac{f_1(\tau_i)}{f_0(\tau_i)} \right]. \tag{8}$$

Equation (8) contains the information about both PDFs $f_1(\cdot)$ and $f_0(\cdot)$. Unfortunately, for underdamped JJs, an exact closed form of these PDFs is still unknown. We have seen in Figs. 2 and 3 that there are regimes in which both the densities follow, with a good approximation, an exponential law. As anticipated, in this case the SM detector is nearly optimal. Indeed, it is straightforward to see that for exponential distributions the decision statistic in Eq. (7) becomes

$$\mathcal{A}(\boldsymbol{\tau}) = \frac{1}{N} \sum_{i=1}^{N} \tau_i \mathop{\substack{\mathcal{H}_1 \\ > \\ < \\ \mathcal{H}_0}} \zeta. \tag{9}$$

We note that if the average escape time under hypothesis $\mathcal{H}_0$ is larger than the same quantity under $\mathcal{H}_1$, the sign in Eq. (9) should be reversed.

In other regimes we estimate both PDFs $f_1(\cdot)$ and $f_0(\cdot)$ using a nonparametric statistical technique such as the kernel density estimation (KDE) [41]. Thus, by means of a large number of samples τ_i (5×10^5 trials), obtained via a Monte Carlo simulation of the escape process of Eq. (4), in both cases $S_0 = 0$ and $S_0 \neq 0$ we retrieve a tight estimate $\widehat{f_j}(\cdot)$ of the unknown PDFs $f_j(\cdot)$. Further details about the KDE are given in Appendix A.

We are now in a position to compute the receiver operator characteristic (ROC) of the test statistic, that is, the plot of P_f vs P_m for different values of ζ [42]. A ROC example is presented in Fig. 5, in which the trade-off between the two error probabilities is evident. To simplify the performance analysis of the detector, we consider the intersection between the ROC and the bisector of the first quadrant angle, which is very close to the point of the ROC curve with the minimum distance to the axis origin. At this point $P_f = P_m$, and we can unambiguously define the error probability P_e that is representative of the detector behavior. The main advantage of this formulation resides in its simplicity and, in many cases, it is also a good approximation of the minimum Bayesian error probability when the prior probabilities of the two hypotheses $\mathcal{H}_0$ and $\mathcal{H}_1$ are considered equal. The error probability P_e gives a rigorous assessment of the detector's performance, and can be related to the heuristic Kumar-Caroll index d_{KC} by an inequality, as elucidated in Appendix B.
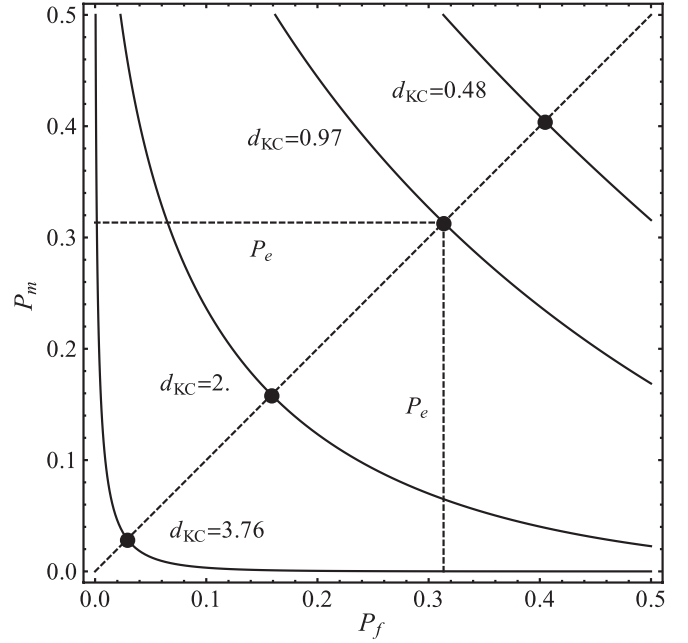

FIG. 5. Typical ROCs of a JJ-based detector under the hypothesis of complete parameter knowledge for different values of d_{KC} (i.e., of ε). Other relevant simulation parameters are $\gamma = 0.3$, $\alpha = 0.05$, and $\varepsilon_N = 0.07$. Moreover, when the signal is present, $\varphi_0 = 0$ and $\omega = 0.8$.

B. Escape time acquisition strategies

The signal-to-noise mixture can be applied to the JJ in different ways [29] to acquire the escape time sequence $\boldsymbol{\tau} = \{\tau_i\}_{i=1}^{N}$. Indeed, when the JJ switches to the running state (see Fig. 1) it is necessary to shield the junction from the signal to reset the static state and to apply the signal again. There is a variety of methods to reset the system. If the frequency of the signal is perfectly known it is in principle possible to reapply the signal always with the same initial phase. This acquisition strategy is called coherent detection. Application again of the signal with the same initial phase involves loss of some fraction of the signal waiting for the correct time to restart the process. In fact the correct initial times read

$$t_i^{(r)} = \frac{2\pi}{\omega} \left\lceil \frac{\omega \tau_i}{2\pi} \right\rceil + t_{i-1}^{(r)}.$$

With this acquisition method the escape PDF shows a striking dependence on φ_0, as elucidated in Fig. 4.

Another possibility, if the frequency is unknown, is to reapply the signal with any phase it might have after the reset procedure, and therefore with an essentially random initial value of φ_0 (incoherent strategy). The PDF of the escape time obtained in this case, essentially the average over φ_0 of the escape densities computed in the coherent strategy case, loses much of the information carried by the initial phase.

C. Filter bank strategy and phase estimation

In the detection theory briefly summarized above, the involved parameters are supposed to be known: the LRT method can be employed only if the signal is supposed to have a known phase. Unfortunately in real scenarios this condition

is rarely fulfilled, and the PDF of the escape times should be considered a function of an unknown parameter vector $\boldsymbol{\theta}$. It is necessary to properly manage the lack of information about $\boldsymbol{\theta}$ to contrive a detection rule that minimizes the deterioration of the performances for unknown parameters. In this section we show how one can retrieve with a filter bank some information about the phase of the signal. The main problem arises because the signal itself might be present or not, and therefore one cannot employ a simple maximum likelihood procedure to determine the best guess for the parameter value. Two popular approaches to the detection with an unknown parameter are currently used in signal processing: the *averaged* LRT (ALRT) and the *generalized* LRT (GLRT). The ALRT, based on the Bayesian theory, consists in averaging the likelihood ratio on the unknown parameters over the density functions corresponding to all the values of the unknown parameter; the resulting best guess is then employed in a Neyman-Pearson criterion to decide the signal presence. The GLRT estimates the unknown parameters via a maximum likelihood approach to select a single most likely phase. This phase is substituted in the PDF expression of the LRT to decide about the signal presence.

In this paper, as a paradigmatic example, we suppose that the unknown parameter is the initial phase, i.e., $\boldsymbol{\theta} = \varphi_0$. Without any *a priori* information, the ALRT approach is substantially equivalent to application of the incoherent acquisition strategy. Unfortunately (as is shown below) this approach loses too much information about the signal presence. Thus we focus on the GLRT, which can be implemented via a filter bank (see Fig. 6 for a pictorial scheme). The filter bank jointly performs the estimation and the detection of the unknown parameter φ_0. In a preliminary step we should determine a sampling of the relevant parameter space $\{\varphi_0^{(i)}\}_{i=1}^{M}$ such that it suitably covers the interval $[-\pi, \pi]$. Each detector of the bank LRT$_i$, tuned on the value $\varphi_0^{(i)}$ and designed as described in Sec. III A, elaborates the sequence of escape times $\boldsymbol{\tau}$ that are acquired with a coherent strategy to obtain a vector of likelihood ratios $\{\Lambda(\boldsymbol{\tau}, \varphi_0^{(i)})\}_{i=1}^{M}$. We recall that the phase φ_0, as depicted in Fig. 4, influences the PDF of $\boldsymbol{\tau}$ *only* when the signal is present. Thus the maximization of the likelihood

under $\mathcal{H}_1$ coincides with maximizing $\Lambda(\boldsymbol{\tau}, \varphi_0)$, and the test (7) becomes

$$\max_{i=1,\ldots,M} \left[\Lambda(\boldsymbol{\tau}, \varphi_0^{(i)}) \right] \underset{\mathcal{H}_0}{\overset{\mathcal{H}_1}{\underset{<}{\gtrless}}} \zeta. \tag{10}$$

The value of $\varphi_0^{(i)}$ that maximizes $\Lambda(\cdot)$ constitutes an estimate of the initial phase,

$$\widehat{\varphi}_0 = \arg \max_{i=1,\ldots,M} \left[\Lambda(\boldsymbol{\tau}, \varphi_0^{(i)}) \right]. \tag{11}$$

To optimize the performance of such a strategy, one should design the filter bank with the appropriate choice of both the number M of the detectors and the values $\varphi_0^{(i)}$. We propose to place the values $\varphi_0^{(i)}$ uniformly spaced in $[-\pi, \pi]$ for the sake of simplicity. Also, we have considered that the JJ behavior for a particular phase value is not too different from that for another one [29]. The number M should be determined recognizing that few detectors offer a poor precision in phase estimation and in detection effectiveness, while too many detectors significantly increase the false alarm probability. A more precise analysis of the bank needed to quantitatively balance the two sides is out of the scope of this paper.

IV. SIMULATION AND NUMERICAL RESULTS

In this section we present extensive Monte Carlo simulations that show the behavior of a detector based on a JJ. As evident in Eq. (7), the LRT employs a fixed number N of escape times and it is *optimal* (in the Neyman-Pearson sense) under this condition. On the other hand the time interval T_{obs} needed to collect N escape times is random and strongly depends on both the signal properties and the JJ parameters. Indeed, when the signal is absent (hypothesis $\mathcal{H}_0$), the mean value of the escape times $\mu_0 = E[\tau|\mathcal{H}_0]$, which is a function of γ, α, and ε_N, reads

$$E[T_{\text{obs}}|\mathcal{H}_0] = N\mu_0. \tag{12}$$

We observe that in the presence of small signals also the escape rate remains roughly unchanged, $\mu_1 = E[\tau|\mathcal{H}_1] \simeq \mu_0$.

To perform a fair comparison under different operative conditions, we fix the mean time interval under the $\mathcal{H}_0$ hypothesis and use the corresponding number of escape times, N. This strategy guarantees a mean duration time of the acquisition stage in any practical situation ($\mathcal{H}_0$ and $\mathcal{H}_1$). Moreover, while the mean time of T_{obs} increases linearly with N, its standard deviation is proportional to $\sqrt{N}$, so the dispersion around the mean value becomes less significant for increasing values of N.

Equation (12) is strictly true only for incoherent acquisition. Indeed, in the coherent case we have to add to μ_0 the mean time needed to assure that the incoming signal is applied to the JJ with the same initial phase. So the approximate relation

$$E[T_{\text{obs}}|\mathcal{H}_0] \approx \begin{cases} N\left(\frac{2\pi}{\omega}\right), & \mu_0 \leqslant \frac{\pi}{\omega}, \\ N\left(\mu_0 + \frac{\pi}{\omega}\right), & \mu_0 > \frac{\pi}{\omega}, \end{cases} \tag{13}$$

reveals that the normalized frequency ω also influences the observation time. We have proven by numerical simulations
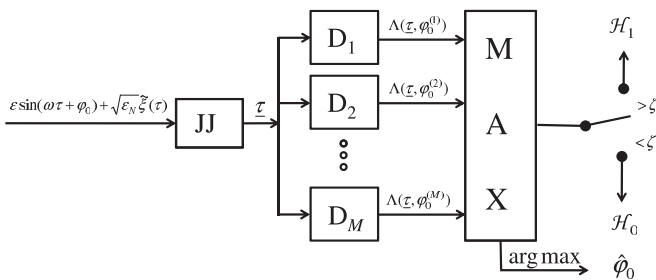

FIG. 6. Schematic of the filter bank. The JJ block indicates the physical device giving the escape time, while the D_i blocks represent the filter bank in which the elements are tuned on different values of the unknown parameter (in this case the initial phase φ_0). The maximization block (MAX) output is compared with a suitable threshold ζ to perform the decision test while arg max gives the maximum likelihood phase estimation.
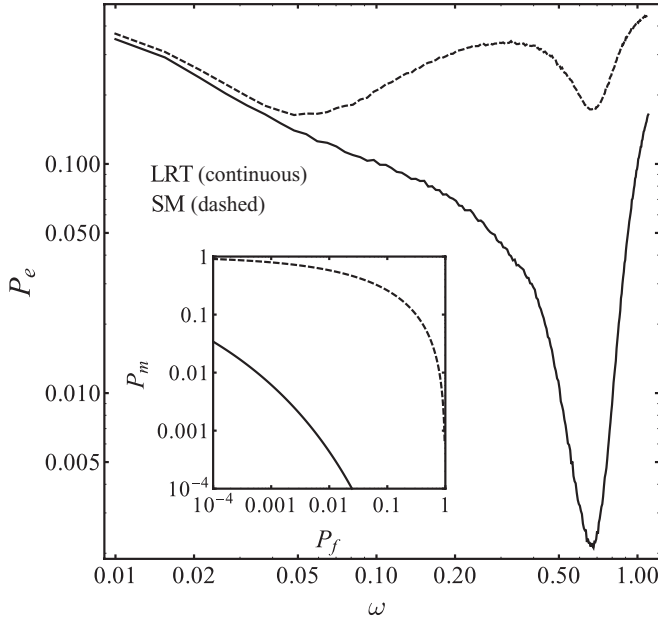
FIG. 7. Detection probability as a function of the applied signal frequency. Parameters of the system are $\gamma = 0.8$, $\alpha = 0.05$, $\varepsilon_N = 0.0175$, $\varepsilon = 0.05$, and $\varphi_0 = 0$. The simulations are performed setting the mean observation time under $\mathcal{H}_0$, $E[T_{obs}|\mathcal{H}_0] = 2000$. Inset: ROCs computed for both the detectors at a frequency close to geometric resonance, $\omega_{res} \approx \omega = 0.7$.

(not shown here) that this effect is negligible (in the interesting range of parameters), so we use the simple approximate Eq. (13) in the remaining part of the paper.

A. LRT performance improvements and signal frequency analysis

In this section we investigate the dependence of the error probability P_e as a function of the normalized signal frequency ω, while in the next section we carefully analyze the dependence of the performance upon the junction parameters. The distinction is somewhat artificial, inasmuch as the normalized frequency ω also depends upon the junction parameters: $\omega = \Omega/\omega_j = \Omega/[2eI_c/(\hbar C)]^{1/2}$. However, in view of some emerging physical and signal detection properties, we prefer to focus on the analysis of the signal frequency and phase in this section, and postpone the analysis of the other junction parameters.

The dependence of the detection properties upon the signal frequency is shown in Fig. 7, where we compare the SM of escape times (broken lines) with the more refined LRT (solid line). We also show in the inset the ROCs of both the tests at a single frequency. In spite of the approximations used to obtain Eq. (8) the improvements of the LRT detection performances are significant. Along the bisector of the inset to Fig. 7 the probability of dismissal P_m decreases by a factor $\simeq 10^2$ from the simple average to the LRT. Since the two curves are computed for the same signal duration, one can also deduce that the LRT allows for a decrease of $\simeq 10^4$ of the signal length with the same false alarm level. It is also evident from Fig. 7 that for all driving frequencies the LRT overperforms the SM detector. Both strategies share a pronounced dip at the
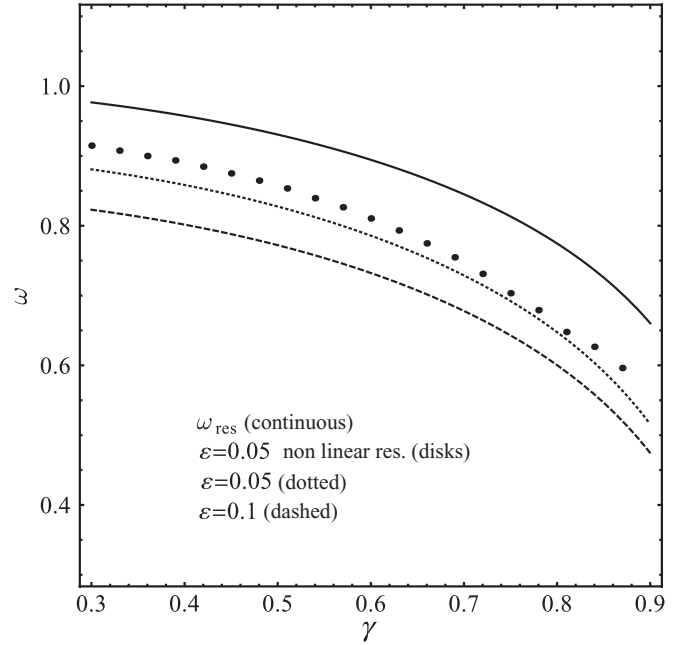

FIG. 8. Frequency ω where a minimum of P_e occurs as a function of the bias current γ for LRT detection strategy. Dashed line refers to a signal with $\varepsilon = 0.1$ and a noise with $\varepsilon_N = 0.07$, and dotted line to $\varepsilon = 0.05$ and a noise with $\varepsilon_N = 0.0175$ (see also Fig. 10). For the sake of comparison we also show (continuous line) the resonant frequency of Eq. (14) corresponding to vanishingly small ε and the nonlinear deterministic resonance curve (circles) in the case $\varepsilon = 0.05$. Other relevant parameters of the system are $\alpha = 0.05$ and $\varphi_0 = 0$. The simulations are performed setting the mean observation time under $\mathcal{H}_0$, $E[T_{obs}|\mathcal{H}_0] = 2000$.

geometric resonance. This frequency is not exactly ω_j, for the tilted washboard potential of Eq. (5) exhibits a dependence of the resonant frequency upon the bias current of the type [32]

$$\omega_{res} \simeq (1 - \gamma^2)^{1/4} \qquad (14)$$

that is mirrored in the performances of the detector. The resonant condition Eq. (14) is obtained through linearization of Eq. (4) for small signal amplitude $\varepsilon = S_0/I_c$. For finite signal amplitude the oscillations explore the nonlinear part of the curvature that is not captured by the second-order Taylor expansion behind Eq. (14). The correction, or rectification effect, accounts for the deviation from Eq. (14) of the resonant frequency at finite signal amplitude, $\omega_{res} = \omega_{res}(\varepsilon)$. In Fig. 8 is shown the nonlinear JJ plasma resonance curve [43]; the higher-order deterministic correction of the plasma frequency approaches the optimal working frequency for detection. The displayed nonlinear plasma frequency is the stable branch in the regime where the resonance curve becomes a multivalued function of the frequency [44]. As a consequence we speculate that best detection performances are attained in the strongly nonlinear distortion regime. In our opinion this result mirrors the similar findings of Ref. [45] concerning the location of the best amplification region in the parameter space. It is noteworthy that such a frequency optimization refinement is needed to ensure that the detector's resonance matches the signal frequency. We conclude the analysis of the geometric resonance by affirming that both SM and LRT detectors

exhibit the dependence predicted by Eq. (14); there exists a suitable neighborhood of ω_{res} that is one of the best regions for detection purposes, with a small correction for the finite signal amplitude.

The SM strategy reveals that a second interesting region occurs at a lower normalized signal frequency, where another resonance appears. The position of this resonance dip depends upon the phase and the temperature [29]; see Figs. 7, 9(a), and 10(a). In fact in Ref. [29] it has been found that a region of optimal detection is pinpointed if the potential well barrier (tuned by γ), the normalized signal frequency ω (the signal frequency Ω divided by the Josephson frequency ω_j), and the noise intensity D are connected by the relation

$$
\omega_{SR} = \frac{\Omega_{SR}}{\omega_j} = \frac{\mu_0}{2\pi C(\varphi_0)} \exp\left\{\frac{2I_c^2}{\omega_j D}\left[\sqrt{1 - \left(\frac{I_B}{I_c}\right)^2}\right.\right.
$$
$$
\left.\left. - \frac{I_B}{I_c}\cos^{-1}\left(\frac{I_B}{I_c}\right)\right]\right\}. \tag{15}
$$

Below the stochastic resonance frequency the PDFs (in both hypotheses) are very similar to those reported in Fig. 2, while above that frequency the PDF (under $\mathcal{H}_1$) develops oscillations similar to those reported in Fig. 3. This explains the disappearance of stochastic resonance (15) in the LRT detection framework, for the LRT exploits the PDF oscillations and does not deteriorate above the frequency (15). Thus the paradoxical increase of the performances at higher noise level for the SM is solved by the observation that the improvement obtained at the ω_{SR} frequency is outperformed by the choice of a more refined LRT detection strategy that takes into account the PDF oscillations. In fact (see Fig. 7), the SM detector performances are always worse than the LRT ones, confirming the general idea that stochastic resonance is a consequence of a suboptimal detection scheme [8]. The practical consequence is that synergetic effects leading to stochastic resonance between noise and signal in nonlinear devices can only be exploited in suboptimal strategies, while in optimal detection strategies noise should be reduced only as much as the experimental setup allows.

B. Physical considerations on JJ parameter optimization

In this section we study the detector performance as a function of JJ parameters. Furthermore, we transform the results obtained with simulations of the normalized Eq. (4) and analyzed with the methods of Sec. III into prescriptions for the physical parameters of an actual JJ. The system depends upon four normalized parameters that can be tuned, with an appropriate choice of the JJ physical parameters, to obtain the best performances. The JJ features that can be modified are as follows:

(1) The Josephson frequency $\omega_j = [2eI_c/(\hbar C)]^{1/2}$ (and hence the capacitance C and the critical current I_c) selects the time scale of the device and must be chosen to maximize the performance of the device. One should compromise between two different requirements: fast to speed up the detection, but still slow enough to allow the available electronics to properly work. The critical current is typically constraint in the range $1\ \mu\text{A} \leqslant I_c \leqslant 10\ \text{mA}$, while the capacitance is in the range 1–1000 pF. The two quantities are not fully independent, for

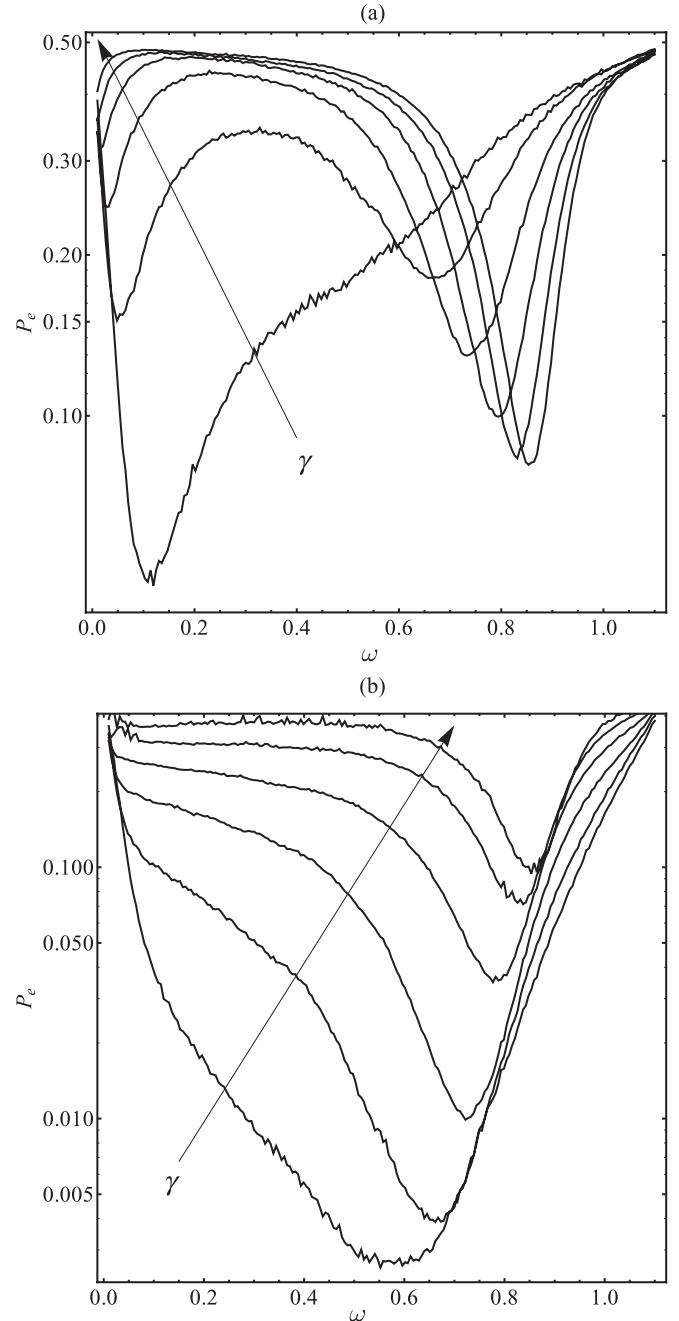FIG. 9. Multiple plot of the error probability P_e as a function of the applied signal frequency ω and the bias current γ. (a) SM detector; (b) LRT detector. Along the arrow, the bias γ decreases from 0.9 to 0.4 with step size -0.1. Other relevant parameters of the system are $\alpha = 0.05$, $\varepsilon_N = 0.0175$, $\varepsilon = 0.05$, and $\varphi_0 = 0$. The simulations are performed setting the mean observation time under $\mathcal{H}_0$, $E[T_{\text{obs}}|\mathcal{H}_0] = 2000$.

both depend upon the distance between the superconducting electrodes and the junction area. The critical current can also be decreased by an external magnetic field. Typically, the available range of ω_j is about 10–1000 GHz.

(2) The applied physical current I_B can be assumed positive (for the symmetry of the problem a negative bias value would just invert the phenomena) and below the critical current to
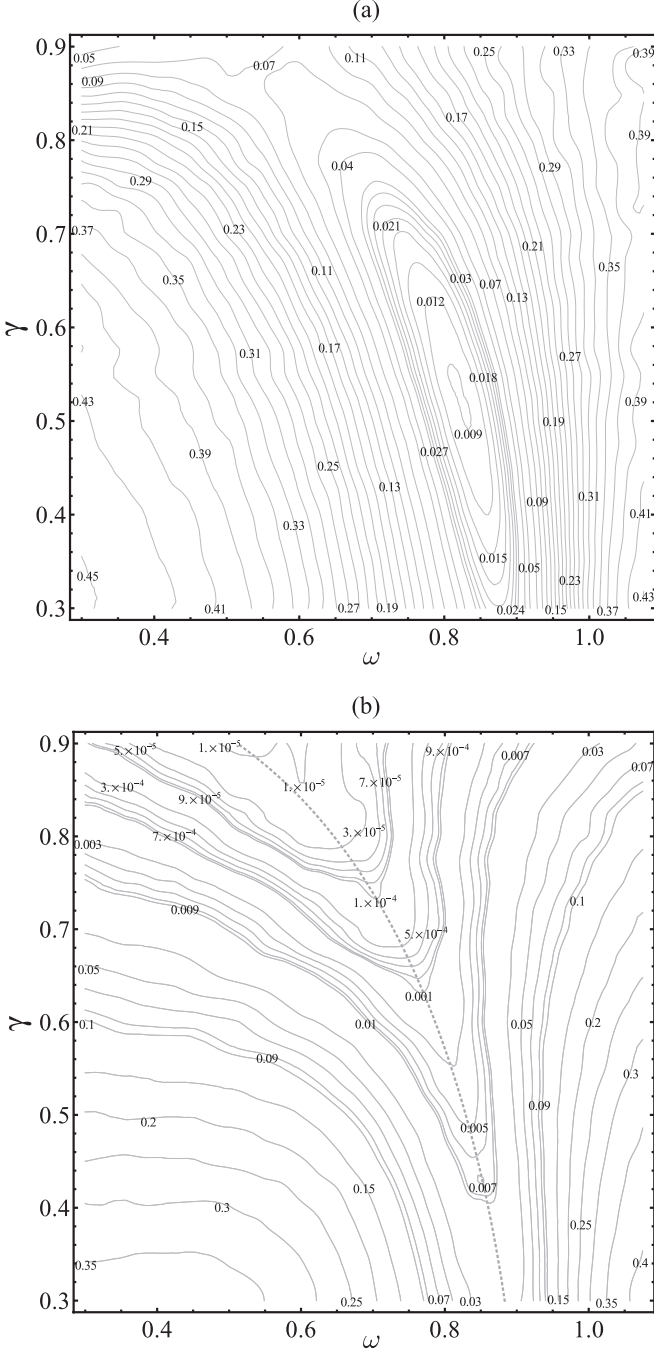
(a)

(b)

FIG. 10. Contour plot of the error probability P_e as a function of the applied signal frequency ω and the bias current γ. (a) SM detector; (b) LRT detector. Thick line in (b) indicates the location of minimum P_e probability. Other relevant parameters of the system are $\alpha = 0.05$, $\varepsilon_N = 0.0175$, $\varepsilon = 0.05$, and $\varphi_0 = 0$. The simulations are performed setting the mean observation time under $\mathcal{H}_0$, $E[T_{\text{obs}}|\mathcal{H}_0] = 2000$.

have two solutions [see Eq. (5)], $0 \leqslant I_B \leqslant I_c$. In normalized units the interval reads $0 \leqslant \gamma \leqslant 1$.

(3) The applied signal amplitude S_0 cannot be amplified without introducing a further noise component. It is therefore convenient to set instead the critical current to have the more appropriate $\varepsilon = S_0/I_c$ normalized signal. It is worth noticing that the normalized intensity of the noise $\varepsilon_N = \omega_j D/I_c^2$ also

depends upon the critical current I_c, and can therefore also be tuned, while obviously the SNR, proportional to $\varepsilon/\sqrt{\varepsilon_N} = S_0/\sqrt{\omega_j D}$, cannot. As already mentioned the critical current of a Josephson junction is typically constrained in the range $1 \, \mu\text{A} \leqslant 10 \, \text{mA}$, and therefore it is not possible to freely choose the normalized signal amplitude. Also, it is important to notice that if the critical current I_c is used to tune the value of the normalized signal, the system frequency ω_j can still be modified via the capacitance C.

(4) The resistance R sets dissipation through the normal electron channel, parallel to the tunnel Josephson element. Dissipation enters in Eq. (4) through the normalized parameter $\alpha = (\omega_j/RI_c)(\hbar/2e)$. The resistance is constrained, inasmuch as the product $I_c R$ depends upon the material: $I_c R = \Delta/2e$. The energy gap Δ for type I traditional superconductors is in the range of meV. The normalized parameter α is limited in the interval $0 < \alpha < 1$. The lower value is due to physical reasons (all quantities are positive), while the upper value is necessary to have a so-called hysteretic junction with two states (detection depends upon the possibility of detecting the switch between these two states). Actual values for viable JJs are narrowed in the range $0.001 \leqslant \alpha \leqslant 0.1$, while the range $0.1 \leqslant \alpha \leqslant 1$ corresponds to the moderately damped regime where retrapping occurs, making it difficult to detect the escape from the static solution [46]. Finally, dissipation can be increased by shunting the junction with an external resistor.

One can interpret the physical parameters R, C, I_c, and I_B and the corresponding normalized parameters α, ω, ε, and γ in the following way. The normalized frequency $\omega = \Omega/\omega_j$ can be chosen to drive the JJ with the most appropriate (for signal detection) frequency, and this sets the ratio of the critical current I_c and capacitance C. The bias current γ, which can be varied through the external bias current I_B, sets the potential well of the system [see Eq. (5)], while the resistance R can be adjusted to have the most appropriate value of dissipation.

As shown in Sec. IV A the normalized frequency plays a major role in the performance; see Figs. 9(a) and 9(b). A detector should therefore be optimized through an appropriate choice of the normalized applied frequency ω. This may be done by tuning the Josephson angular velocity close to the signal frequency. Therefore we conclude that signals in the range of ω_j are suitable for detection with JJs, while slower or faster signals are poorly analyzed with this technique.

Once the system is optimized in frequency, probably the most easily tunable parameter is the external bias current I_B, which affects the normalized bias γ. In the geometric resonance neighborhood, as shown in Fig. 10(a), there is a clear optimal point around $\gamma \simeq 0.5$ for the SM technique. The physical interpretation is that the average escape time is most sensitive to the external signal when the bias current γ, and hence the energy barrier of Eq. (5), is intermediate between the maximum ($\gamma = 0$) and the minimum barrier ($\gamma = 1$). Indeed, in the former case there are few escape events in the observation time, while in the latter case the escape is dominated by noise and the average is little affected by the signal. It is interesting to see that for some high values of γ the stochastic resonance dip around ω_{SR} performs better than the geometric resonance close to ω_{res}. The LRT, as expected, performs better than the SM for all γ values; see Figs. 10(a)

and 10(b). The LRT detector also shows a different behavior, namely, the larger the bias current the more accurate the estimate, as displayed in Figs. 9(b) and 10(b). The qualitative explanation is as follows: with a more accurate analysis of the escape times it is possible to recognize the presence of the signal embedded in the noise even when the average is little affected by the signal itself, due to the optimal exploitation of the PDFs information—see Eq. (7). It is important to notice that practical detectors cannot be realized just by setting the bias current $\gamma = 1$ for several reasons. First, the metastable state exists only for $\gamma < 1$. Second, in the analysis presented here we assume that the escape time is measured with an infinite accuracy. In practical detectors the finite error associated with the measurements is more relevant for shorter escape times. We conclude that simulations suggest use of a bias current I_B as close to I_c as possible (i.e., $\gamma \simeq 1$), providing that the resulting escape times are still measurable with good accuracy. This entails that the limit of the performances is given by the actual electronics employed.

The critical current might be chosen to change the normalized drive amplitude $\varepsilon = S_0/I_c$ and the noise intensity $\varepsilon_N = \omega_j D/I_c^2$. As anticipated, the available range of the critical current is relatively narrow. However, we have found that a unifying parameter assumes the role of γ (which depends upon the bias and can therefore be easily tuned) and ε_N. Physical intuition suggests that escape time detector performances are mainly dependent on the potential barrier ΔU and the noise intensity ε_N. A realistic guess could be that a relevant parameter is the ratio ρ:

$$\rho = \frac{\Delta U(\gamma)}{\varepsilon_N} = \frac{2[\sqrt{1 - \gamma^2} - \gamma \cos^{-1}(\gamma)]}{\varepsilon_N}. \quad (16)$$

The simulations in Fig. 11 (which display the contour level of error probability as a function of $\Delta U/\varepsilon_N$ and ω for two different values of ε keeping the same SNR proportional to $\varepsilon/\sqrt{\varepsilon_N}$) confirm this conjecture. Despite the nonlinear character of the system, the two contour plots are qualitatively similar. The main difference is due to the rectification effect (see again Fig. 8). We conclude that the analysis of the parameter ρ leads to the same qualitative optimization recipes as for parameter γ: for the LRT strategy, the normalized bias current should be close to unity, while for the SM strategy optimization requires an intermediate bias value.

Concerning dissipation, simulations with different values α in the underdamped regime ($\alpha \leqslant 0.1$) lead to the following result: with reduced dissipation the escape rate is increased, and therefore more events can be collected in the same time interval. As a consequence, the lower the dissipation the better the detector performance. So we conclude that one should try to use a junction resistance as large as possible to decrease dissipation. Moreover, our findings (lower dissipation favors detection) indicate that an external shunt to decrease the junction resistance might result in worse performance. Let us summarize the findings of the best JJ parameters for signal detection:

(1) The normalized frequency $\omega = \Omega/\omega_j$ shows best performances around the geometrical resonance of Eq. (15), $\omega \simeq \omega_{res}$, for both LRT and SM. JJs are therefore best suited for signals whose frequency can be around 10–1000 GHz. If

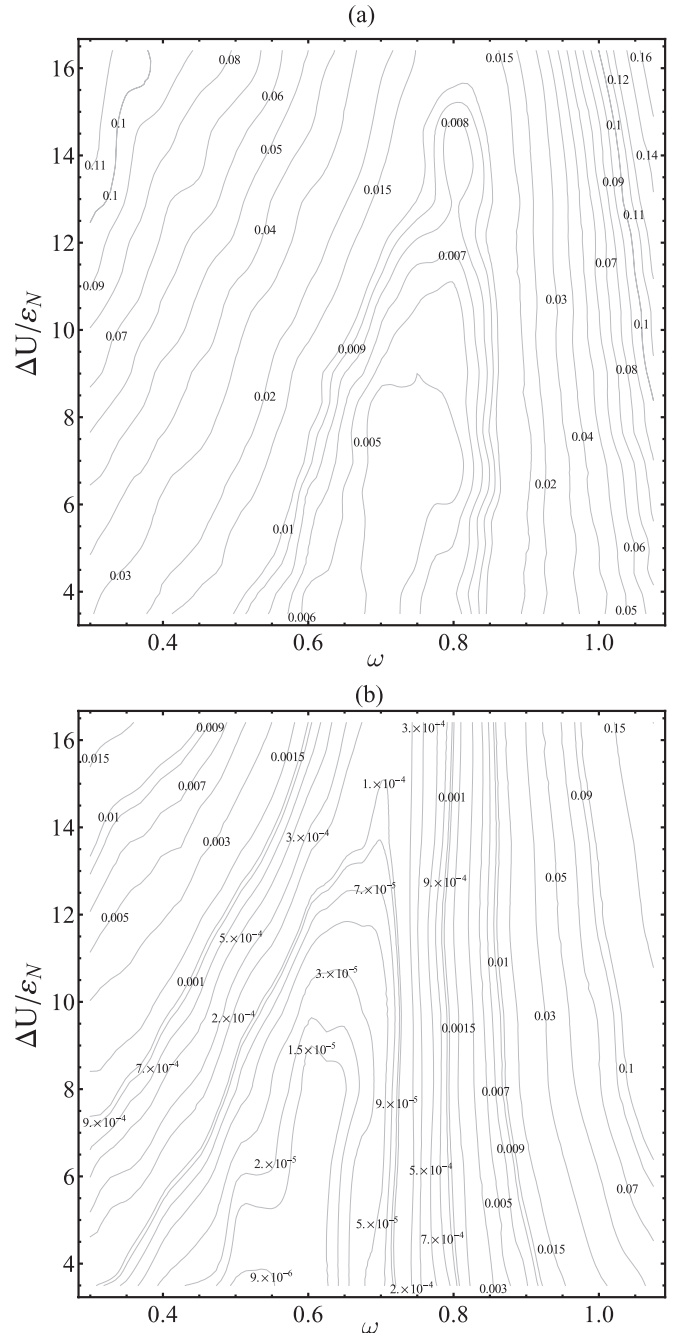FIG. 11. Contour plot of the error probability P_e as a function of the applied signal frequency ω and the noise-normalized barrier $\Delta U/\varepsilon_N$. (a) $\varepsilon = 0.1$ and $\varepsilon_N = 0.07$; (b) $\varepsilon = 0.05$ and $\varepsilon_N = 0.0175$. Other relevant parameters of the system are $\alpha = 0.05$ and $\varphi_0 = 0$. The simulations are performed setting the mean observation time under $\mathcal{H}_0$, $E[T_{obs}|\mathcal{H}_0] = 2000$.

the simpler sample mean is employed, a second local optimum appears at a lower frequency, Eq. (15), a frequency that can also be much smaller than the geometric resonance.

(2) The bias current for the LRT strategy should be set as close as possible to $\gamma = I_B/I_c = 1$ to achieve the lowest value of ΔU; see Fig. 9(b). For the SM strategy the currents should be set at an intermediate value that depends on the ratio ρ between the energy barrier and the signal.

(3) The normalized signal ε_N is not an independent variable, for the relevant parameter is the ratio between the normalized signal and the energy barrier, Eq. (16). This ratio should be, for the LRT strategy, as small as possible; this is automatically set if the bias current condition has been fulfilled.

(4) The normalized dissipation parameter α should be as low as possible. A low dissipation in fact results in faster escapes, thus increasing the statistics at a fixed length of the signal. The other features (in terms of optimization of the normalized drive frequency, bias current, and signal amplitude) are independent of dissipation. We do not show the numerical results for different α, for they are very similar to the displayed results obtained with $\alpha = 0.05$.

The search for optimal parameters has led to qualitative indications (e.g., the indication for high bias and matching to the nonlinear resonance) for selection of the experimental setup without actually repeating our numerical work. The purpose of the previous analysis is to determine the optimal working point location in the JJ parameter space at a fixed value of the SNR. On the other hand, the SNR strongly affects the performance of the detector evaluated through the error probability. Thus it is interesting to characterize the relationship between the SNR and the error probability P_e for both SM and LRT detectors. Our ansatz is that the performances measured by the KC index follow the power law

$$d_{KC}(Y) \sim A(Y) \left(\frac{\varepsilon}{\sqrt{\varepsilon_N}} \right)^{\eta(Y)}, \qquad (17)$$

where Y is a general asymptotically Gaussian decision statistic. In our setup Y is replaced by the average of the sampled escape times, $\mathcal{A}(\boldsymbol{\tau})$, for the SM detector and by $\Lambda(\boldsymbol{\tau})$ for the LRT detector, defined in Eqs. (9) and (8), respectively. Therefore, as described in Appendix B, the error probability can be expressed as

$$P_e = \frac{1}{2} \mathrm{erfc} \left[B(Y) \left(\frac{\varepsilon}{\sqrt{\varepsilon_N}} \right)^{\eta(Y)} \right]. \qquad (18)$$

The behavior for the optimal detection parameters has been verified via numerical simulation and the results are shown in Fig. 12(a). It is evident that the model fit in Eq. (18) is well suited for both SM and LRT detectors. More interesting is that the scaling law, i.e., the value of $\eta(Y)$, is different for the two detection strategies. Indeed, for the SM detector we have found $\eta(\mathcal{A}) = 1.63 \approx 3/2$ Ref. [29], while the LRT shows a scaling law ruled by $\eta(\Lambda) = 0.97 \approx 1$, which is nearly optimal, because it is also the behavior of the exponent for the ideal matched filter [as can be promptly seen in Fig. 12(b)]. This striking difference between the SM and LRT is even more evident on the basis of the following consideration. The KC index is roughly proportional to $\sqrt{T_{\mathrm{obs}}}$ via the coefficient $B(Y)$; hence on lowering the SNR the detection time should be extended to preserve the same detector performance. To keep constant the quality of the detection, the observation time T_{obs} should increase as $(\varepsilon/\sqrt{\varepsilon_N})^{-3}$ for the SM detector and as $(\varepsilon/\sqrt{\varepsilon_N})^{-2}$ for the LRT one. Such a different scaling gives a huge advantage to the LRT in the challenging case of small SNR. In Fig. 12(b) the comparison between the proposed LRT detection scheme and matched filter [30] is
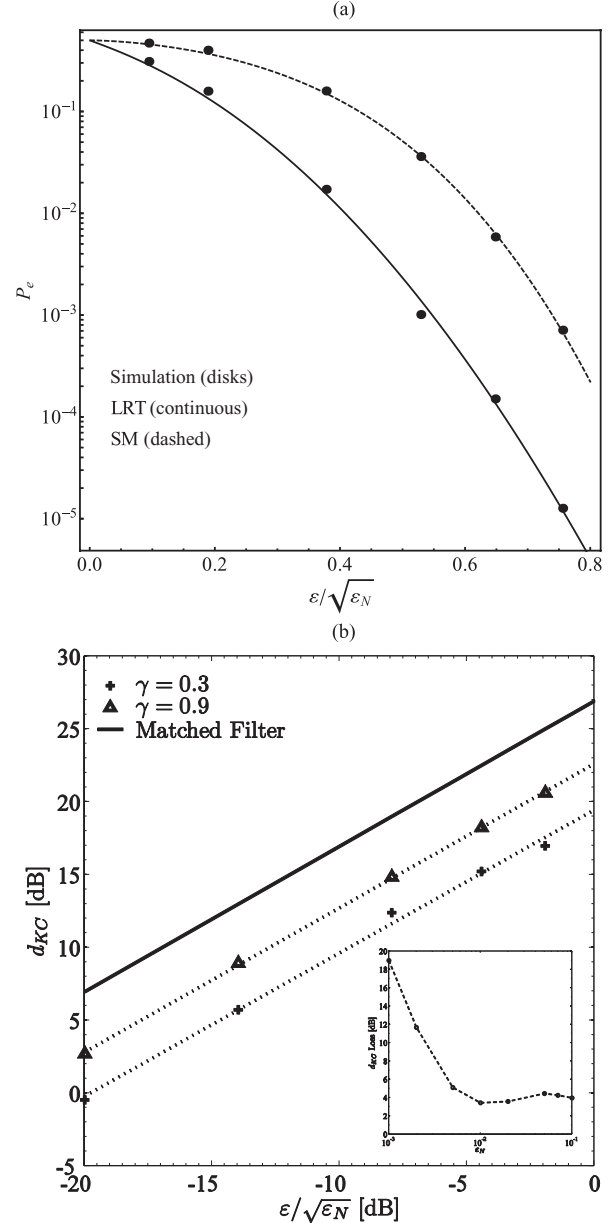

FIG. 12. (a) Error probability P_e as a function of $\varepsilon/\sqrt{\varepsilon_N}$ (related to the SNR). Disks are obtained by numerical simulations; continuous lines are computed by fitting the data using the KC approximation in Eq. (18). The parameters used in the simulations are $\gamma = 0.3$, $\alpha = 0.05$, and $\varepsilon_N = 0.07$. Moreover, when the signal is present, $\varphi_0 = 0$ and $\omega = 0.8$, close to the optimal detection point ω_{res}. (b) KC index (reported in dB) of proposed LRT strategy (for different parameters $\gamma = 0.3$, 0.9, and ω near the optimal detection frequency) vs the same SNR-related parameter compared with the KC index of the matched filter (best available strategy). Inset: d_{KC} loss with respect to matched filter (on a dB scale) for $\gamma = 0.9$ as a function of ε_N ($\varepsilon/\sqrt{\varepsilon_N}$ is fixed to -20 dB). In all cases simulations are performed with $E[T_{\mathrm{obs}}|\mathcal{H}_0] = 2000$.

further elucidated by using a suitable representation based on the KC index. In this framework, as anticipated, the $\eta(\Lambda)$ parameter is readily seen to be of the order of unity for all displayed curves. Moreover, it is simple to quantify the loss in decibels (dB) of the detector performance, by mean of the

straight line intercepts, which for the best case is nearly 4 dB. Rephrasing of this loss in terms of the ratio between LRT and matched filter observation time (for continuous signals) corresponds to a factor ~ 2.5. Such a speed-up factor can be achieved by frequency scaling and/or parallel very-large-scale integration implementation of the detector, and JJs could turn out to be competitive in practical applications. In the inset of Fig. 12(b) the d_{KC} loss is shown with respect to a matched filter on a decibel scale as a function of the noise parameter ε_N. The LRT, as expected, never passes the matched filter. The minimal loss is reached for reasonably high values of ε_N that correspond to the physical limit of negligible escapes toward the higher local minima. Finally, we have verified that inside the optimality region this function is substantially independent of the time window T_{obs} and of the ratio $\varepsilon/\sqrt{\varepsilon_N}$.

C. Unknown phase estimation and signal detection

As anticipated in Sec. III C, an incoherent strategy may be implemented with an acquisition method that requires a simpler measurement setup. In Fig. 13 three different ROCs are displayed to compare the proposed detection strategies. The figure shows the natural behavior, i.e., that the best detection performances are obtained with the LRT detector (solid curve). A filter bank (GLRT coherent strategy shown as the dashed curve) results in an acceptable deterioration of the detector performance. As anticipated, due to the huge reduction of information on the initial phase the incoherent

FIG. 14. Variance of the maximum likelihood estimate of φ_0 as a function of the number N of escape times. Continuous line is obtained by Monte Carlo method; dashed line is the theoretical Cramer-Rao lower bound. Inset: A typical probability mass function estimate (with 10^5 trials) of the unknown parameter φ_0 by using only $N = 10$ samples. The signal is generated with an initial phase $\varphi_0 = 0$. Other relevant parameters are $\gamma = 0.5$, $\alpha = 0.05$, $\varepsilon_N = 0.07$, $\varepsilon = 0.1$, and $\omega = 0.8$, close to the optimal detection point ω_{res}.

strategy outperforms the other strategies. The dependence of the variance estimate φ_0 obtained with the GLRT detector implemented via filter bank is illustrate in Fig. 14. The $M = 100$ sampling points are placed in $\varphi_0^{(i)} = \frac{\pi}{M}(2i - 1 - M)$ in order to cover the interval $[-\pi, \pi]$. The sinusoidal signal with known parameters $\varepsilon = 0.1$, $\omega = 0.8$, and $\varepsilon_N = 0.07$ is applied to a JJ with $\alpha = 0.05$ and $\gamma = 0.5$.

The unknown parameter $\varphi_0 = 0$ is chosen in the middle position between two sampling points, the worst case for the filter bank performance [47]. Figure 13 also shows (continuous curve) that the variance is reduced by increase in the number N of escape times (the acquisition is supposed coherent). In particular the estimator variance reaches the Cramer-Rao lower bound relative to the escape time statistics, i.e., the asymptotic efficiency [31], for $N \sim 50$ escapes. The proposed estimator is therefore able to effectively extract the information about the initial signal phase φ_0 carried by the escape times. Of course, when for very large values of N the expected variance becomes lower than the discretization error $(2\pi/M)^2/12$, the latter dominates and causes a saturation of the performance.
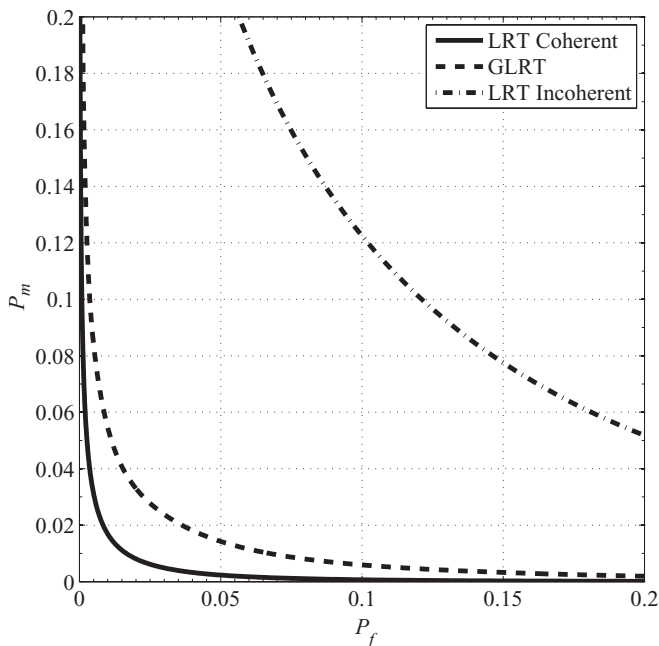

FIG. 13. ROCs computed for three different detectors: LRT detector based on incoherent acquisition of escape times (dot-dashed line), filter bank coherent acquisition (GLRT) detector (dashed line), and LRT detector based on coherent data (continuous line). For all strategies we ensure the same mean observation time under $\mathcal{H}_0$ (i.e., $E[T_{\text{obs}}|\mathcal{H}_0] \approx 1500$). Other relevant parameters are $\gamma = 0.5$, $\alpha = 0.05$, and $\varepsilon_N = 0.07$. Moreover, when the signal is present, $\varepsilon = 0.1$, $\varphi_0 = 0$, and $\omega = 0.8$, close to the optimal detection point ω_{res}.
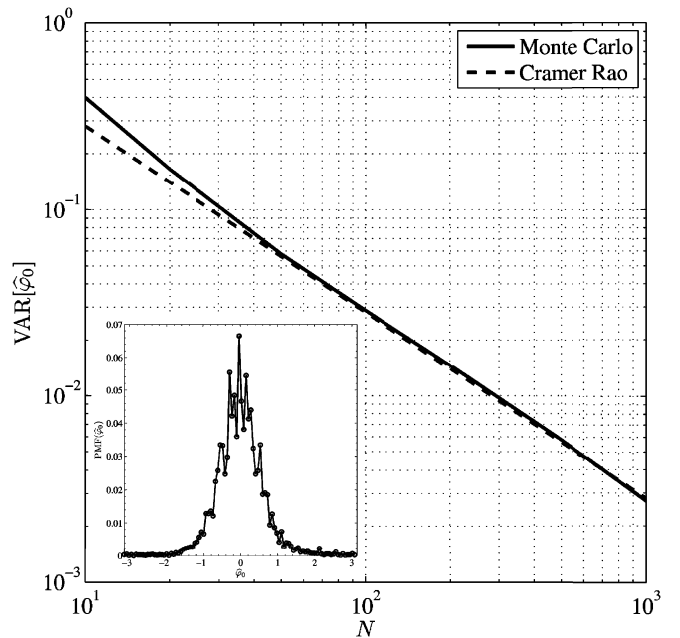
V. CONCLUSIONS

We have investigated a case of detection of sinusoidal signals by means of a nonlinear device, namely, an underdamped JJ. Some warnings are in order to clarify the limits of the approach. First, compared to traditional methods, JJs require cryogenic facilities to cool the superconducting electrodes. Second, the best performances are obtained at high frequency,

thus requiring the handling of microwaves without introducing distortions or undesirable noise increases. Third, we recall that a matched filter is the optimal method for signal detection, and therefore our proposal can be considered only when such an optimal method is not available because of technical difficulties. Fourth, we underline that the improvements are obtained at the price of heavier numerical work, since the escape time distribution is not theoretically known.

We have shown that the analysis of the escape times, an experimentally accessible quantity, can be performed through an intuitive approach, the estimate of the average, or with a more refined likelihood-based statistic. The latter analysis leads to a significant improvement of the performance of the LRT with respect to the SM, greatly reducing the error probability. The advantages of better detectors could result in solid improvements in terms of experimental time length and costs.

We have found that the conditions that favor detection (in terms of frequency, bias current, and dissipation) depend on the adopted strategy (SM or LRT). Moreover, we have found that the likelihood ratio test unexpectedly leads to an optimal scaling law for small SNR. This result is surprising, because the signal detection has been doubly deteriorated by the insertion of a nonlinear device and the change of the observable variable (i.e., escape time instead of the original signal-noise mixture). We have also shown that the LRT approach is scalable to detector arrays, thus allowing a signal phase estimate. However, we believe that the most important finding is that, in some sense, the experimental setup should be tailored to the data analysis. Indeed, the two detection approaches cannot be optimized with the same normalized frequency and applied bias current. We speculate that the above results are fairly common to other activation detectors, because our analysis mostly relies on an Arrhenius-like activation law, which is independent of the details of the energy barrier. It is therefore possible that the advantages can be exploited, generalizing to other systems the methods we present in this work.

Future research will be devoted to the use of signal processing tools for thermally induced and quantum-assisted transition rate discrimination [18]. This difference is particularly difficult to detect because a microwave source in a JJ in the macroscopic quantum tunneling regime produces multiple photon quantum transitions that can be confused with subharmonic excitations due to nonlinear JJ behavior [48].

APPENDIX A: KERNEL DENSITY ESTIMATION

The likelihood ratio test, presented in Eq. (6), requires a complete knowledge of the PDFs $f_0(\cdot)$ and $f_1(\cdot)$ for both the hypothesis. As already mentioned, unfortunately there is no theoretical result that can provide this knowledge. Thus we are compelled to use an estimated version of these PDFs. A simple but effective strategy is to use the kernel density estimation

[41]. This technique generalizes the basic idea of histogram by using a so-called *kernel function* $K(\cdot)$ that usually is a symmetric PDF. If there is a random sample $X = \{X_i\}_{i \in [1,N]}$, where N is the sample size, the kernel estimator should be

$$\widehat{g}(x) = \frac{1}{Nw} \sum_{i=1}^{N} K\left(\frac{x - X_i}{w}\right), \tag{A1}$$

where the parameter w is the *bandwidth* (also called the *smoothing parameter*). If we apply this framework to escape times, we immediately encounter a first difficulty. Indeed, the escape times are by definition positive, i.e., their PDFs, under the generic hypothesis $\mathcal{H}_j, j \in \{0,1\}$, have the property

$$f_j(t) = 0, \quad \forall t < 0. \tag{A2}$$

Equation (A1) leads to an estimated PDF that does not satisfy the inequality (A2). To deal with this issue, the following procedure has been applied.

(a) For a fixed hypothesis $\mathcal{H}_j$, the random sample of escape times $\boldsymbol{\tau} = \{\tau_i\}_{i \in [1,N]}$ is transformed via

$$X = \ln(\tau). \tag{A3}$$

Thus we deal with the random sample $X = \{X_i\}_{i \in [1,N]}$ that can assume every value on the real axis.

(b) By means of Eq. (A1), an estimated PDF $\widehat{g}_j(x)$ is computed.

(c) The PDF $\widehat{f}_j(t)$ is obtained from $\widehat{g}_j(x)$ via

$$\widehat{f}_j(t) = \frac{\widehat{g}_j(\ln(t))}{t}, \quad t > 0. \tag{A4}$$

The procedure described above has to be applied twice, i.e., under both the hypotheses $\mathcal{H}_j$, to obtain the PDF estimates $\widehat{f}_0(\cdot)$ and $\widehat{f}_1(\cdot)$. Then, when we have to decide about the presence of a signal via an independently generated random sample of escape times, we can compute the statistic in Eq. (7) as

$$\widehat{\Lambda}(\boldsymbol{\tau}) = \frac{1}{N} \sum_{i=1}^{N} \ln\left[\frac{\widehat{g}_1(\ln(\tau_i))]}{\widehat{g}_0(\ln(\tau_i))}\right] \mathop{\gtrless}_{\mathcal{H}_0}^{\mathcal{H}_1} \zeta. \tag{A5}$$

The procedure is completely specified if in Eq. (A1) one chooses both the kernel function and the bandwidth. We have used the kernel defined by a standard Gaussian density, i.e.,

$$K(t) = \frac{1}{\sqrt{2\pi}} \exp\left(-\frac{t^2}{2}\right).$$

This kernel is rewarding, for the estimated density is smooth and there are no subsets on the real axis with zero density. The latter point is essential in the likelihood ratios to avoid singularities. The drawback is in a little loss in estimation performances, which is negligible for the sample size used ($\sim 5 \times 10^5$). The smoothing parameter selection, instead is a hard task. Indeed, it is known (see, Ref. [41]) that the optimal choice has the form

$$w = C(K, f) N^{-1/5}, \tag{A6}$$

where $C(K, f)$ is a constant that depends on the used kernel $K(\cdot)$ and, unfortunately, on the same density $f(\cdot)$ to be estimated. Thus we have used a simple closed form obtained

when both $K(\cdot)$ and $f(\cdot)$ are Gaussian, that is,

$$w = \left(\tfrac{4}{3}\right)^{1/5} \widehat{\sigma} N^{-1/5}, \tag{A7}$$

where $\widehat{\sigma}$ is the sample standard deviation of the data set. This choice is near optimal for unimodal densities, which is the case when the $\mathcal{H}_0$ hypothesis is in force, while it leads to some oversmoothing for multimodal densities that arise under the $\mathcal{H}_1$ hypothesis. Also in this case the large sample used helps us make the oversmoothing negligible. Moreover, the slight oversmoothing introduced under $\mathcal{H}_1$ can only worsen the LRT test performance, because the PDF oscillations, which contain the largest part of additional information with respect to the sample mean, are underestimated.

APPENDIX B: KUMAR-CARROL INDEX

In this Appendix we introduce the general concept of the KC index and its connection with a more effective parameter: the error probability. In the context of decision theory, the main purpose is to discriminate between two hypotheses: signal is present ($\mathcal{H}_1$) vs signal is absent ($\mathcal{H}_0$). Let Y be the selected decision statistics, expressed as a function of the escape time vector $\boldsymbol{\tau}$, which has to be compared with a suitable threshold ζ. Moreover, suppose that $\mu_1(Y)$ and $\mu_0(Y)$ are the averages of the decision statistic under the two hypotheses (subscripts 1 and 0 refer to the presence and absence of the signal, respectively) while the corresponding standard deviations are denoted with $\sigma_1(Y)$ and $\sigma_0(Y)$. The KC index can be accordingly defined as

$$d_{KC}(Y) = \frac{|\mu_1(Y) - \mu_0(Y)|}{\sqrt{\frac{1}{2}\left[\sigma_1^2(Y) + \sigma_0^2(Y)\right]}}. \tag{B1}$$

In this paper both the decision statistics can be modeled as the sample mean of a suitable random variable, i.e., τ for

the SM and $\mathcal{L}$ for the LRT detector [see Eqs. (9) and (7), respectively]. In this case both the statistics, for large sample size, are asymptotically normal due to the central limit theorem [49]. Therefore the error probability P_e (defined above as the value of the ROC $P_m = P_f$) can be expressed as

$$P_e = \frac{1}{2}\mathrm{erfc}\left(\sqrt{1 + \frac{\Delta(Y)^2}{4}} \frac{d_{KC}(Y)}{2\sqrt{2}}\right), \tag{B2}$$

where $\Delta(Y) = 2|\sigma_0(Y) - \sigma_1(Y)|/|\sigma_0(Y) + \sigma_1(Y)|$. By inspection it can be shown that Eq. (B2) is a decreasing function of Δ, and therefore by neglecting the difference among standard deviations (if it exists) it is possible to retrieve an upper bound of P_e that is a function of d_{KC} only, i.e.,

$$P_e \leqslant \frac{1}{2}\mathrm{erfc}\left(\frac{d_{KC}(Y)}{2\sqrt{2}}\right). \tag{B3}$$

The inequality (B3) clarifies the heuristic character of the KC index as an indicator of the detector performance. The concept introduced above can be applied to SM and LRT detectors, by setting $Y := \mathcal{A}(\tau)$ and $Y := \Lambda(\tau)$, respectively. Under the hypothesis that a power law relationship between the KC index and the SNR exists, as exemplified by

$$d_{KC}(Y) \sim A(Y)\left(\frac{\varepsilon}{\sqrt{\varepsilon_N}}\right)^{\eta(Y)}, \tag{B4}$$

the error probability can be expressed as

$$P_e = \frac{1}{2}\mathrm{erfc}\left[B(Y)\left(\frac{\varepsilon}{\sqrt{\varepsilon_N}}\right)^{\eta(Y)}\right], \tag{B5}$$

where $B(Y) = \sqrt{1 + \frac{\Delta(Y)^2}{4}} A(Y)/(2\sqrt{2})$. This last equation has been used to interpret the relationship between P_e and $\varepsilon/\sqrt{\varepsilon_N}$ in Sec. IV; see Fig. 12.

[1] A. R. Bulsara and A. Zador, Phys. Rev. E **54**, R2185 (1996).

[2] T. Novotný, J. Stat. Mech. (2009) P01050.

[3] M. I. Dykman and M. A. Krigovlaz, Sov. Phys. JETP **50**, 30 (1979).

[4] R. Graham and T. Tél, Phys. Rev. Lett. **52**, 9 (1984); Phys. Rev. A **31**, 1109 (1985).

[5] M. I. Dykman, B. Golding, L. I. McCann, V. N. Smelyanskiy, D. G. Luchinsky, R. Mannella, and P. V. E. McClintock, Chaos **11**, 587 (2001).

[6] I. Goychuk and P. Hänggi, Eur. Phys. J. B **69**, 29 (2009).

[7] M. E. Inchiosa and A. R. Bulsara, Phys. Rev. E **53**, R2021 (1996).

[8] V. Galdi, V. Pierro, and I. M. Pinto, Phys. Rev. E **57**, 6470 (1998).

[9] M. H. Devoret, J. M. Martinis, and J. Clarke, Phys. Rev. Lett. **55**, 1908 (1985).

[10] M. H. Devoret, D. Esteve, J. M. Martinis, A. Cleland, and J. Clarke, Phys. Rev. B **36**, 58 (1987).

[11] Y. Yu and S. Han, Phys. Rev. Lett. **91**, 127003 (2003).

[12] S. Poletto, F. Chiarello, M. G. Castellano, J. Lisenfeld, A. Lukashenko, C. Cosmelli, G. Torrioli, P. Carelli, and A. V. Ustinov, New J. Phys. **11**, 013009 (2009).

[13] G. Carapella and G. Costabile, Phys. Rev. Lett. **87**, 077002 (2001).

[14] J. Tobiska and Yu. V. Nazarov, Phys. Rev. Lett. **93**, 106801 (2004).

[15] J. P. Pekola, T. E. Nieminen, M. Meschke, J. M. Kivioja, A. O. Niskanen, and J. J. Vartiainen, Phys. Rev. Lett. **95**, 197004 (2005).

[16] B. Huard, H. Pothier, Norman O. Birge, D. Esteve, X. Wainta, and J. Ankerhold, Ann. Phys. (Leipzig) **16**, 736 (2007).

[17] A. Barone, F. Lombardi, G. Rotoli, and F. Tafuri, Low Temp. Phys. **36**, 876 (2010).

[18] J. A. Blackburn, M. Cirillo, and N. Grønbech-Jensen, Phys. Lett. A **374**, 2827 (2010).

[19] Y. Levinson, Phys. Rev. B **67**, 184504 (2003).

[20] K. Mitra, C. J. Lobb, and C. A. R. Sá de Melo, Phys. Rev. B **79**, 132507 (2009).

[21] A. D. Hibbs, A. L. Singsaas, E. W. Jacobs, A. R. Bulsara, and J. J. Bekkedahl, J. Appl. Phys. **77**, 2582 (1995).

[22] M. D. Mittleman, *Sensing with Terahertz Radiation* (Springer, Berlin, 2003).

[23] P. Jaranowski, A. Krolak, and B. F. Schutz, Phys. Rev. D **58**, 063001 (1998).

[24] R. Benzi, A. Sutera, and A. Vulpiani, J. Phys. A **14**, L453 (1981).

[25] B. McNamara and K. Wiesenfeld, Phys. Rev. A **39**, 4854 (1989).

[26] C. R. Doering and J. C. Gadoua, Phys. Rev. Lett. **69**, 2318 (1992).

[27] X. X. Wang and J. D. Bao, Phys. Rev. E **83**, 011127 (2011).

[28] A. Fiasconaro and B. Spagnolo, Phys. Rev. E **83**, 041122 (2011).

[29] G. Filatrella and V. Pierro, Phys. Rev. E **82**, 046712 (2010).

[30] C. W. Helstrom, *Statistical Theory of Signal Detection* (Pergamon, Oxford, 1968).

[31] J. Shao, *Mathematical Statistics* (Springer, New York, 2003).

[32] A. Barone and G. Paternò, *Physics and Application of Josephson Effect* (John Wiley, New York, 1982).

[33] E. Ben-Jacob and D. J. Bergman, Phys. Rev. A **29**, 2021 (1984).

[34] H. Risken, *The Fokker-Planck Equation: Methods of Solution and Applications* (Springer, Berlin, 1989).

[35] M. H. Devoret, J. M. Martinis, D. Esteve, and J. Clarke, Phys. Rev. Lett. **53**, 1260 (1984).

[36] R. Mannella, in *Stochastic Processes in Physics, Chemistry and Biology*, edited by J. A. Freund and T. Pöschel (Springer, Berlin, 2001), p. 353.

[37] B. V. K. V. Kumar and C. W. Carroll, Opt. Eng. **23**, 732 (1984).

[38] L. Gammaitoni, F. Marchesoni, E. Menichella-Saetta, and S. Santucci, Phys. Rev. Lett. **62**, 349 (1989).

[39] P. Silvestrini, S. Pagano, R. Cristiano, O. Liengme, and K. E. Gray, Phys. Rev. Lett. **60**, 844 (1988).

[40] N. Berglund and B. Guentz, Europhys. Lett. **70**, 1 (2005).

[41] B. W. Silverman, *Density Estimation for Statistics and Data Analysis* (Chapman and Hall/CRC, 1998).

[42] The receiver performance here named ROC is sometimes also called detection error tradeoff.

[43] T. Hanaguri, Y. Tsuchiya, and A. Maeda, Phys. Rev. B **58**, R8929 (1998).

[44] L. D. Landau and E. M. Lifshitz, *Mechanics* (Pergamon, New York, 1976).

[45] S. Wahlsten, S. Rudner, and T. Claeson, J. Appl. Phys. **49**, 4248 (1978).

[46] J. C. Fenton and P. A. Warburton, Phys. Rev. B **78**, 054526 (2008).

[47] We recall that, although the phase is unknown, in the coherent strategy each detector is strobed by using the signal period. This ensures that we keep the initial (unknown) phase constant. Had we chosen the incoherent strategy, we would have lost all information about the phase.

[48] T. Bauch, T. Lindstro, F. Tafuri, G. Rotoli, P. Delsing, T. Claeson, and F. Lombardi, Science **311**, 57 (2006).

[49] P. Billingsley, *Probability and Measure* (John Wiley, New York, 1995).